

Single voltage-gated calcium channel current in rat neocortical layer 5 pyramidal neurons in physiological calcium: voltage ramp fluctuation analysis

Christian Scheppach^{1,2} and Hugh P.C. Robinson¹

¹Physiological Laboratory, Department of Physiology, Development and Neuroscience, University of Cambridge, CB2 3EG, UK.

²Institute of Physics, University of Freiburg, Hermann-Herder-Str. 3, D-79104 Freiburg, Germany

Additional information

Running title: Physiological single calcium channel current in cortical neurons

Key words: voltage-gated calcium channels, fluctuation analysis, calcium spike

Table of contents category: Neuroscience – cellular/molecular

Corresponding author: Hugh P.C. Robinson, Physiological Laboratory, Department of Physiology, Development and Neuroscience, University of Cambridge, Downing Street, Cambridge, CB2 3EG, UK. Email: hpcr@cam.ac.uk

Abbreviations

CrP, creatine phosphate; HVA, high-voltage activated; L5, layer 5; LVA, low-voltage activated; PSD, power spectral density.

Key points

- Voltage-gated calcium channels (VGCCs) are essential for the function of neurons, participating in signalling both pre- and post-synaptically.
- The single channel current amplitude of VGCCs is extremely small and challenging to estimate when recording in a physiological concentration of extracellular calcium (1-2 mM). However, it is a key parameter for calcium signalling.
- To estimate single open channel current, we carried out fluctuation analysis of VGCC currents in nucleated patches. A novel approach, validated by modelling, was used, based on an analysis of ramp depolarization responses, which is particularly suited to voltage-gated calcium channel data.
- At a membrane voltage of -25 mV, the single channel current was 0.07 pA (equivalent to about 200 ions per millisecond) in 2 mM extracellular calcium – considerably smaller than some previous estimates.
- The results are relevant to understanding stochastic effects in calcium signalling, e.g. dendritic calcium spikes, and to calcium nanodomains.

Abstract

Voltage-gated calcium channels (VGCCs) are present in all mammalian central neurons, controlling presynaptic release of transmitter, postsynaptic signalling and synaptic integration. The amplitudes of their single open-channel currents in a physiological concentration of extracellular calcium, however, are not well determined, being too small to resolve directly in patch-clamp recordings. However, measurement of this quantity is essential for estimating numbers of functional VGCCs in the membrane and the size of channel-associated calcium signalling domains, and for understanding the stochastic nature of calcium signalling. Here, we recorded the voltage-gated calcium channel current in nucleated patches from layer 5 pyramidal neurons in rat neocortex, in physiological external calcium (1-2 mM). The pharmacological profile of the current was consistent with R-type or Q-type channels, and a small L-type component. In order to reliably separate the calcium current fluctuations from other background currents for

fluctuation analysis, despite their small amplitude and rapid rundown, we developed a method using band-pass filtered current responses to ramp membrane potential stimulation. We validated the accuracy of the method by analysing simulated data. At external calcium concentration of 1 mM, and a membrane potential of -20 to -15 mV, we found that single channel current amplitude was about 0.04 pA, increasing to 0.065 pA at 2 mM external calcium, and 0.12 pA at 5 mM. The relaxation time constant of the fluctuations was in the range 0.2–0.8 ms. The results demonstrate that single channel current amplitude of native voltage-gated calcium channels can be resolved accurately and straightforwardly.

Introduction

Voltage-gated calcium channels (Hille, 2001; Catterall *et al.*, 2005; Tsien & Barrett, 2005) are central to many physiological processes, and are present in most neuronal membranes, where they have important roles in signalling. The apical dendrites of neocortical layer 5 (L5) pyramidal neurons (Spruston, 2008; Stuart *et al.*, 2008) exhibit action potentials carried by Ca^{2+} (Schiller *et al.*, 1997). These dendritic Ca^{2+} spikes provide an amplification mechanism for distal synaptic inputs, triggering bursts of sodium action potentials at the soma and hence constitute a fundamental mechanism of synaptic integration in these neurons (Larkum *et al.*, 2009; Major *et al.*, 2013). Similar dendritic calcium spikes have been found in hippocampal CA1 pyramidal cells, and Purkinje neurons. At presynaptic terminals, calcium influx through voltage-gated calcium channels triggers the vesicular release of neurotransmitter (Südhof, 2013).

Eleven subtypes of the principal channel-forming α_1 subunit have been described, distinguished by electrophysiological and pharmacological properties and grouped in three gene families (Catterall *et al.*, 2005). The first family Ca_v1 , encodes L-type channels, while Ca_v2 genes encode N-type, splice variants P- and Q-type, and R-type channels, and the Ca_v3 genes encode T-type channels. Ca_v1 and Ca_v2 channels require higher depolarisations to activate than Ca_v3 channels. The former are therefore called high-voltage activated (HVA) calcium channels, and the latter low-voltage activated (LVA).

The amplitude of currents through native single Ca^{2+} channels at physiological extracellular Ca^{2+} concentrations (1-2 mM, Jones & Keep, 1988) is a key parameter. Knowing it is essential to be able to relate the density of functional channels to the size of whole-cell calcium currents, to characterise the stochasticity of calcium signalling due to random opening and closing of single ion channels (Chow & White, 1996; Cannon *et al.*, 2010; Anwar *et al.*, 2013), and to understand the formation of calcium nanodomains, highly localised and concentrated plumes of calcium on the cytoplasmic side of open calcium channels, allowing specific signalling (Weber *et al.*, 2010), which depends on the rate of Ca^{2+} entry through individual channels. Calcium channels also have interactions with $\alpha_2\delta$ and β subunits and are subject to extensive modulation, which can greatly modify channel properties in a cell-type-specific manner. Therefore, it is particularly important to study the properties of native calcium channels in neurons, as opposed to simplified expression systems. However, physiological single Ca_v channel current has not been extensively investigated, with only a few estimates in the literature (Fenwick *et al.*, 1982; Gollasch *et al.*, 1992; Weber *et al.*, 2010; Church & Stanley, 1996). In chick dorsal root ganglion neurons, Weber *et al.* estimated values of 0.24 pA (Ca_v1), 0.33 pA (Ca_v2) and 0.2 pA (Ca_v3), at a membrane potential of -65 mV and an extracellular calcium concentration of 2 mM, by direct single-channel recording and extrapolating from measurements at more elevated calcium concentrations. Such a small amplitude makes it extremely challenging to resolve and estimate accurately. Single calcium channels are therefore studied almost exclusively in high extracellular barium solutions (e.g. Fox *et al.*, 1987a), since barium permeates Ca_v1 and Ca_v2 channels at higher rates than does calcium, giving much larger, detectable channel current amplitudes close to 1 pA in size.

Here, we have applied fluctuation analysis (Stevens, 1972; Neher & Stevens, 1977; Sigworth, 1977, 1980) on population Ca_v currents in low-noise, space-clamped recordings, in nucleated patches isolated from L5 pyramidal neurons, in order to estimate the effective single channel current of native Ca_v channels under physiological conditions. By a novel method of separation of the currents activated during ramp depolarizations and band-pass filtering, which we validated by modelling, we were able to isolate Ca_v channel current fluctuations, even in the face of significant run-down of the channel current (a common problem in the study of Ca^{2+} channels, see Bean, 1992;

Almog & Korngreen, 2009). We estimated a value of 0.065 pA at -20 to -15 mV and 2 mM extracellular calcium, predicting that about 200 channels are open at the peak of inward macroscopic calcium currents in somatic nucleated patches.

Methods

Tissue preparation

Animal procedures adhered to U.K. Home Office legislation and University of Cambridge guidelines. Acute brain slices were obtained from Wistar rats aged 6-14 days. Animals were killed by dislocation of the neck, and parasagittal brain slices were prepared as detailed in Davie *et al.* (2006). The brain was cut along the midline and one hemisphere was glued by the medial surface to a tilted block (12°) on top of the horizontal slicer stage, slightly raising the ventral part of the brain. 300 μ m thick slices were obtained with a vibratome (Leica VT1200S), with the dorsal cortical surface facing the horizontal blade. Slices were incubated at 34°C for 30 min and then kept at room temperature.

Solutions, drugs, chemicals

Extracellular solution (used for slicing and perfusion of slices) had the following composition: 125 mM NaCl, 2.5 mM KCl, 2 mM CaCl_2 , 1 mM MgCl_2 , 1.25 mM NaH_2PO_4 , 25 mM NaHCO_3 , 25 mM glucose, bubbled with carbogen gas (95% O_2 , 5% CO_2), pH 7.4 (c.f. Sakmann & Neher, 1995 p.200; Stuart & Sakmann, 1994; Davie *et al.*, 2006). Intracellular Cs-based pipette solution had the following composition: 90 mM Cs-methanesulfonate, 30 mM CsCl, 10 mM BAPTA- Na_4 (Ca^{2+} chelator), 11 mM HEPES buffer, to which was added 4 mM ATP (ATP Mg salt obtained from Sigma; free Mg: about 1 mM), 0.3 mM GTP (GTP Na salt hydrate obtained from Sigma; 1.2 mM Na^+), and 10 mM creatine phosphate (CrP) Na_2 (Na CrP dibasic tetrahydrate obtained from Sigma), to mitigate run-down of Ca^{2+} channels (Bean, 1992), and pH was adjusted to 7.3 with NaOH and HCl (about 4.5 mM NaOH for HEPES, about 8 mM NaOH for ATP). The liquid junction potential of 12.2 mV was corrected for. HEPES-buffered extracellular solution consisted of: 145 mM NaCl, 2.5 mM KCl, 2 mM CaCl_2 , 1 mM MgCl_2 , 10 mM HEPES, pH adjusted to 7.4 with about 4.2 mM NaOH.

Tetrodotoxin (TTX, Na channel blocker) was obtained from Alomone Labs (“Tetrodotoxin (with citrate)”) and Tocris (“Tetrodotoxin citrate”). Nifedipine (L-type Ca^{2+} channel blocker) was obtained from Sigma. A 40 mM stock solution in ethanol was produced on the day of the experiment. (S)-(-)-Bay K 8644 was obtained from Tocris. A 10 mM stock solution in ethanol was prepared, kept in the fridge and used within two days. ω -Conotoxin GVIA and ω -agatoxin IVA were obtained from Tocris. 100 μl of each blocking drug dissolved in HEPES-buffered extracellular solution was applied with a pipette into the recording chamber, and the bath solution was gently stirred by aspiration with the pipette several times. Since the recording chamber solution volume was around 3 ml, the concentration of the drug was diluted by a factor of about 30.

Recording

Slices were viewed with an Olympus BX50WI fixed stage upright microscope and a x60 objective, or a x10 objective for larger-scale overview, with infrared (IR) or visible light differential interference contrast (DIC) optics and a Luminera Infinity 3M CCD camera. To assist orientation in the slice, the position in the slicing plane was monitored with an optical position encoder (Renishaw), displaying x and y coordinates at micron resolution. Pipette pressure was monitored by a pressure meter. Voltage clamp data were collected with a MultiClamp 700B (Axon Instruments) amplifier, with a feedback resistor of 50 $\text{G}\Omega$ and a 10 kHz 4-pole Bessel filter, with waveform generation and sampling at 16-bit resolution at a frequency of 50 kHz, using a National Instruments analog interface and custom software written in C++ and Matlab. During the experiment, perfusion with extracellular solution was maintained in the recording chamber with a perfusion line and a suction line. All experiments were performed at room temperature (20-23°C).

Pyramidal neurons in cortical layer V were visually identified. In order to minimise variability, cells from the same cortical location were consistently targeted. Slices were always obtained from the right hemisphere. In consecutive parasagittal slices, the orientation of pyramidal cell dendrites changes from slice to slice, and slices in which the dendrites run roughly parallel to the slice surface were selected, which came from about half-way between the midline and the lateral brain surface. The central

part of the cortex in the rostral-caudal direction was targeted, corresponding to the sensory hindlimb region (Paxinos & Watson, 2009).

Patch pipettes were pulled from borosilicate glass capillaries (Harvard Apparatus, 1.5 mm outer diameter, 0.86 mm inner diameter, filamented glass) and fire-polished. Tip resistances (with the Cs-based pipette solution) were between 5.5 and 6.5 M Ω . Nucleated patch recordings were performed as described in Sather *et al.* (1992). A whole-cell recording was obtained, and a negative pressure of about -200 mbar was applied to the pipette, aspirating the cell nucleus to the pipette tip. Maintaining the negative pressure, the pipette was slowly and carefully retracted, such that the nucleus was pulled out of the cell and acted as a place holder around which the cell membrane resealed. The nucleated patch was pulled out of the slice and then raised well above it. Finally, the negative pipette pressure was reduced to about -50 mbar. The process from initial contact of the membrane with the pipette tip to the first recorded sweep took about 4 to 7 minutes.

Ca²⁺ channel currents were recorded during depolarising ramps, e.g. from a holding potential of -70 mV rising to 0 mV (slope 0.6 mV/ms, stimulus repeated every 3 s), and also during depolarising voltage steps (e.g. holding potential -70 mV, 100 ms long steps to test potentials cycling through -80 mV, -60 mV, -30 mV, -20 mV, -10 mV and 0 mV, stimulus repeated every 3 s). In nifedipine block experiments: in 6 of 8 patches, ramp stimulus with a holding potential of -70 mV, prepulse at -90 mV for 200 ms, rise to 0 mV, stimulus repeated every 5 s. In one patch, holding potential of -60 mV, no prepulse, depolarisation to 0 mV, repeated every 2 s. In one patch, holding potential of -70 mV, no prepulse, depolarisation to 0 mV, repeated every 2 s.

Data analysis, modelling and statistics

Analysis was carried out using custom code in MATLAB and R. Leak subtraction for step responses (Fig. 1A) was carried out by subtraction of scaled ensemble-averaged responses to small steps (holding potential \pm 10 mV) below the activation range of the calcium current. All current traces were digitally filtered with a low-pass Gaussian filter (Sakmann & Neher, 1995 p.485) at a -3dB corner frequency $f_c = 1$ kHz. To isolate current fluctuations, ramp currents were fitted with a piecewise polynomial, consisting of a flat segment and two linear segments linked by cubic splines (Fig. 2A), giving a

smooth, continuous-derivative heuristic function whose eight parameters were fitted by minimizing squared deviation from the data, using a Nelder-Mead simplex algorithm (Matlab function `fminsearch`), which was taken as the estimate of the mean current μ_I . Following subtraction of this function, the fluctuating current responses were passed through a high-pass filter, by subtracting from the signal its low-pass-filtered version (Gaussian filter with $f_c = 50$ Hz, resulting in a high-pass filter with corner frequency 94 Hz), to reject extraneous low-frequency noise and error introduced at low frequencies by the mean-fitting procedure. The variance of the resulting band-pass filtered fluctuations (σ_I^2) was computed over brief (5 ms) time bins, and the single channel current i estimated from the relationship $i \approx \sigma_I^2 / \mu_I$ (see Results).

To assess the accuracy of the analysis, synthetic data were generated by convolving Gaussian white noise with an exponential function to produce Lorentzian coloured channel noise, and adding it to the mean current function (see above), scaling the noise in amplitude so that its variance was equal to the product of the single channel current amplitude and the mean current (Equation 2).

Weighted straight-line fits with fit parameter estimates, errors and correlations were obtained with the statistics package R.

Results

Calcium channel currents in nucleated patches

Voltage-gated Ca^{2+} channel currents were recorded in nucleated patches from neocortical L5 pyramidal neurons, using a cesium-based intracellular pipette solution to block potassium channel currents (Bean, 1992), 1 μM TTX in the Ringer solution to block sodium channel currents, and 2 mM extracellular calcium. Figure 1A shows an example family of leak-subtracted currents in response to step depolarizations. The current is activated around -30 mV and has a more pronounced inactivating component as the membrane is depolarised further. The small amplitude of these currents at physiological calcium concentration means that the signal-to-noise ratio is also small. However, in responses to ramp depolarization (Fig. 1B), the onset and voltage-dependence of the current is much clearer, and allows unambiguous identification of the voltage-gated calcium current, abolished completely by application of 200 μM cadmium

(Fig. 1C, $n = 11$ cells). The block could not be reversed by perfusing the bath again with Cd-free solution ($n=2$). Partial block was observed at $20 \mu\text{M Cd}^{2+}$ ($n=2$, not shown), which was reversible ($n=1$). $2 \mu\text{M Cd}^{2+}$ did not block the current ($n=1$). As expected for calcium currents (Bean, 1992; Almog & Korngreen, 2009), despite inclusion of ATP and GTP in the pipette, there was often a relatively fast rundown over the first 5-10 minutes following establishment of the recording.

In most cases (5/8), nifedipine (L-type Ca^{2+} channel blocker) produced no clear blocking effect (fig. 1Di), but a partial block was noted in 3 patches. Generally, a small partial block was difficult to differentiate from the natural time course of rundown. Therefore, the Ca^{2+} channel current was plotted against time (fig. 1D), and if addition of the blocker resulted in a drop of the current below what would be expected from the extrapolated rundown beforehand, the data were interpreted as showing a block. Nifedipine was used at several concentrations: $3 \mu\text{M}$ (2 patches, partial block in 1), $30 \mu\text{M}$ (4 patches, partial block in 1), $50 \mu\text{M}$ (1 patch, partial block) and $70 \mu\text{M}$ (1 patch, no block). Bay K8644 ($1 \mu\text{M}$), an L-type channel agonist, had no discernible effect on the ramp-activated inward current ($n=2$), but boosted the current during depolarising voltage steps ($n=2$). We conclude that some L-type channels are present in somata of L5 pyramidal neurons, but they do not account for the major component of the calcium current. ω -Conotoxin GVIA (N-type Ca^{2+} channel blocker) at $1 \mu\text{M}$ did generally not block the Ca^{2+} channel current (Fig. 1Dii, $n=7$, only in one patch possible slight block). ω -Agatoxin IVA (P-type Ca^{2+} channel blocker, 30 nM) also had no blocking effect (Figure 1Diii, $n=4$).

In conclusion, the full block by Cd^{2+} shows that the inward current observed in ramps is carried by voltage-gated calcium channels. The lack of block by ω -conotoxin GVIA and ω -agatoxin IVA indicates that N and P type channels are not involved, while T-type channels would have a much lower activation threshold (Nowycky *et al.*, 1985), suggesting that the ramp-evoked current corresponds mostly to R-type ($\text{Cav}2.3$), or possibly Q-type ($\text{Cav}2.1$) channels, with a small contribution from L-type channels.

Fluctuation analysis during voltage ramps

Single calcium channel openings at physiological calcium concentrations are effectively impossible to resolve directly, because the combination of their small amplitude and

short open duration means that their signal falls below the noise level of the patch-clamp technique. Therefore, we adopted a fluctuation analysis approach (Stevens, 1972; Neher & Stevens, 1977; Sigworth, 1977, 1980), with the usual assumptions of N identical, independent channels with open probability p , leading to the following relationship of total current variance σ_I^2 to the ensemble mean level of current μ_I :

$$\sigma_I^2 = i\mu_I - \frac{\mu_I^2}{N}, \quad (1)$$

where i is the single channel current (review: Sakmann & Neher, 1995 p.81; Hille, 2001 p.384). If p is small, then

$$\sigma_I^2 \approx i\mu_I. \quad (2)$$

Fluctuation analysis of voltage-gated channels is usually done by measuring channel currents during steps to a constant voltage (Sigworth, 1977, 1980). Current mean and variance are obtained by ensemble averaging a number of consecutive sweeps. However, we found that this approach was not suitable for native voltage-gated calcium currents, because of the rapid time course of rundown: computing a suitable ensemble average relies on complete stability of conditions and number of available channels over a considerable number (at least ≈ 20) of consecutive sweeps. Leak and capacitance current subtraction has to be performed separately, and these currents also need to be constant. Furthermore, if one is interested in the single-channel current over a range of voltages, steps to different test voltages have to be carried out. These factors make conventional fluctuation analysis impractical and unreliable. Instead, we developed a method for extracting fluctuations from fitting an idealized mean time course, similar to the approach used for quantally-varying synaptic currents (Robinson *et al.*, 1991; Traynelis *et al.*, 1993) but applied to ramp-evoked currents.

The leak current was obtained from a straight line fit to the initial part of the ramp response from 5 ms to 40 ms after the start of the ramp (Fig. 1B), corresponding to a potential range of -67 to -46 mV, below the activation range of the calcium current. After subtraction of the linear leak current, each ramp response was fitted by least-squares (see Methods) with a piecewise polynomial function (Fig 2A, see Methods). This heuristic function gave very good fits to current traces (Fig. 2B). We then applied high-pass filtering to the mean-subtracted responses. This step increased the robustness of the measurement, by confining the signal to a bandwidth (94 Hz – 1 kHz) containing a substantial fraction of the channel noise power, while rejecting potentially large

fluctuations of baseline at low frequencies. Secondly, it dealt with the problem that fitting the mean current to each individual ramp response leads to an underestimation of the current variance (see also discussion). Since we subtract from the data not the underlying true mean current, but the fitted mean current, the obtained fluctuation trace is contaminated by their difference. This difference contains only low frequencies and is hence strongly attenuated by the high-pass filter. Fig. 2C shows an example of how the variance of the filtered fluctuations evolves in successive time bins during an individual current response to a voltage ramp.

The drawback of high-pass filtering the fluctuations is that it also removes some of the fluctuation power due to channel gating and therefore the variance must be corrected for this. To that end, we investigated the spectral composition of the fluctuations, so that the effect of filtering could be quantified. We found that the autocorrelation function of the fluctuations was well-fitted by a single exponential relaxation (Lorentzian frequency component) passed through the same filtering (Fig. 3A), with noise time constant τ in the range 0.2-0.8 ms (Fig. 3B). Fig. 3C illustrates how exponential noise of $\tau = 0.8$ ms (Lorentzian half-power corner frequency = 200 Hz) is filtered. The combined effect of high- and low-pass filtering cuts a substantial amount of the power of channel gating fluctuations, resulting in a correction factor γ by which the current variance is reduced, i.e. $\gamma = \sigma_{\text{filtered}}^2 / \sigma^2$, where $\sigma_{\text{filtered}}^2$ is the experimentally measured, filtered current variance and σ^2 is the full variance of the unfiltered channel current fluctuations. γ is a function of τ (Fig. 3D) and can be calculated by integrating the filtered Lorentzian power spectral density (Fig. 3C) over frequency, and dividing by the total variance. It can be seen that γ is actually rather insensitive to τ , remaining between 0.5 and 0.574 over the measured range of τ . Thus the measured variance is converted to true total variance by dividing by γ .

We assessed the accuracy of this method by benchmarking it with synthetic signals consisting of exponentially-correlated channel noise (see Methods) and Gaussian white baseline noise, added to a mean current function (Fig. 2A) with known parameters. As can be seen in Fig. 3E, the underlying single channel current is correctly recovered over a wide range of values, and the uncertainty for fitting single time bins is quantified. We also used the simulated data to assess the extent of underestimation of fluctuations resulting from fitting the mean current to the data. The current variance was

underestimated by up to 8% (bin 10), but after application of the high-pass filter, the underestimation was reduced to below 0.3%.

Applying this to actual data (Fig. 4) using one patch as an example, the baseline noise variance $\sigma_{\text{baseline}}^2$ was measured in many repeated trials over the 20-40 ms time bin (Fig. 4A), as well as the variance σ_{exptl}^2 in bins 1 to 10 (Fig. 4B,C), and plotted against the mean current in the bins. An error-weighted least-squares fit of the linear relationship $\sigma_{\text{exptl}}^2 = \gamma i \mu_I + \sigma_{\text{baseline}}^2$ was computed. (Since baseline points are calculated from 20 ms segments, they receive four times the weight of the 5 ms test bin points). The fitted slopes γi are plotted as a function of membrane potential in Fig. 4D, revealing that the single channel current has an approximately linear current-voltage relationship.

Dividing by γ to give the final estimates of single channel current, we plot data for 7 patches at three different calcium concentrations in Fig. 5, as a function of membrane potential. Two patches at 1 mM, two patches at 2 mM, and three at 5 mM were analysed, and straight line fits to the single channel current-voltage relationships were calculated for the pooled data at each concentration. Single channel current is reduced with depolarization, with a shallow slope, implying a highly positive reversal potential, as expected, but the relationship may be better approximated by a Goldman-Hodgkin-Katz current equation than an ohmic linear relationship. However, given the limited voltage range of the data, nonlinear extrapolation is not justified. Table 1 summarises the parameters of the fits.

The single channel current is highly sensitive to the extracellular calcium concentration, as expected (Fig. 5). At 1 and 2 mM, in the physiological range, the single channel currents at -40 mV, just above activation are 0.045 and 0.07 pA respectively. At the peak of the inward current, around -10 mV, the corresponding values are 0.04 pA (1 mM) and 0.065 pA (2 mM). This means that approximately 200 channels are open at the maximum of the ramp response.

Discussion

In this study, we aimed to measure the single-channel current of native voltage-gated Ca^{2+} channels in neocortical layer 5 pyramidal neurons, in physiological extracellular

Ca²⁺ concentrations. This is an essential step towards understanding how many channels participate in physiological calcium currents, how variable these currents are, and how the calcium signalling complex of the channel microenvironment operates. In addition, channel properties are modified by accessory proteins, and lipid environment, hence it is important to assess them in native channels *in situ*, rather than in expression systems.

Measuring single channel current amplitude using voltage ramps

Accurate estimation of the physiological unitary amplitude of voltage-gated calcium channels has proved a difficult problem. The concentration of the permeant ion is low (1-1.5 mM), while even in near-isotonic (100-150 mM) barium or calcium, single channel conductance is small (7-25 pS, depending on subtype, see Catterall *et al.*, 2005). Under the assumption of a linear relationship of single channel conductance to the permeant ion concentration, values in the region of 0.007-0.025 pA might be expected with a driving force of 100 mV. With mean channel open times in the millisecond or sub-millisecond range, a bandwidth of at least 1 kHz is required to adequately identify channel openings, at which even in optimal patch-clamp recording conditions (Levis & Rae, 1993) one has to expect at least 20 fA rms noise. Thus direct resolution of the single physiological calcium channel amplitude is, at best, at the extreme limit of what is achievable with the patch-clamp technique. However, this approach has been attempted, by prolonging channel openings pharmacologically, which allows a more aggressive noise reduction by low-pass filtering (Gollasch *et al.*, 1992), or by using low-noise quartz patch pipettes (Weber *et al.*, 2010; Church & Stanley, 1996). Nevertheless, the accuracy of direct single-channel current measurements remains hard to assess (see discussion below, in *Comparison with previous estimates*).

Another possible approach, as we have adopted here, is to analyse the statistics of current fluctuations in a population containing a large number of channels. Indeed, this was used in an early landmark study on single voltage-gated calcium channels (Fenwick *et al.*, 1982). Although fluctuation analysis can in principle measure much lower unitary channel amplitudes, it is important to highlight its limitations. In general, one must assume that all channel openings are identical in amplitude – if not, the single channel current estimate will be an average for the different subtypes of channel

openings, weighted according to their prevalence, although this may still be useful information. Fluctuation analysis also assumes independence of channels in the population – however this is usually a valid assumption. In conventional fluctuation analysis, the expectation current is estimated as the ensemble mean current, by averaging many identical trials. However, this approach has the major drawback of requiring a long period of stationarity, to accumulate at least 20 to 30 responses under identical conditions. We found that this was not realisable in this preparation, and may be a questionable strategy to apply to calcium channels under any circumstances, owing to the progressive rundown to which they are prone, even when ATP and GTP are provided in the patch solution (Bean, 1992; Almog & Korngreen, 2009). Instead, we adapted this method in several ways. First, we took the approach of fitting individual responses to a smooth function which was sufficiently flexible to follow the form of macroscopic currents accurately without over-fitting, i.e. following the time course of fluctuations. This resembles previous fitting methods applied to synaptic currents (Robinson *et al.*, 1991; Traynelis *et al.*, 1993). In both cases, fitting a function by least-squares can result in a slight underestimation of the variance – i.e. the fitted function is closer overall, in a least-squares sense, to the response than is the underlying expectation current. However, this kind of error is reduced by using a reasonably extended trial, essentially allowing time for a high number of fluctuations around the mean within each trial. In the present situation, we found in simulations that the underestimation was up to 8%. Applying a high-pass filter to the fluctuation trace dealt with this problem in a controlled way, reducing the error to below 0.3%. Secondly, the high-pass filter rejected extraneous low-frequency artefacts, which we found to be a useful enhancement to the robustness of the method. We showed how to compensate for this step, taking into account the temporal correlation of the fluctuations (Fig. 3A). Finally, by using a ramp stimulus, we were able to sample the entire voltage range of interest and simplify leak subtraction. We then verified this method by simulation (Fig. 3E), showing that it faithfully recovers single-channel current over the full range of possible values.

We assumed that channel open probability p is small, such that the linear approximation of eqn. (2) is valid. For Ca^{2+} channels, at the voltages of this study (below -18 mV), the channel open probability has been measured to be small, below

0.2 even at the top end of the voltage range (Fox *et al.*, 1987a), such that an error above 10% arising from this source is unlikely. If an ion channel type has larger open probabilities (as would for example be the case for Na channels, see Sigworth, 1977, 1980), the method presented here is not valid. However, it could be extended to the use of the full quadratic relationship (eqn. (1)) for channel types for which this proves necessary.

Pharmacological identification

We concluded that the current which we studied in voltage ramp responses in nucleated patches was likely to be due to high-voltage-activated R- and/or Q-type channels, with a small contribution from L-type channels. Cadmium (200 μM) totally blocked the current. Nifedipine (3-70 μM), an L-type blocker, only resulted in a partial block in some patches, and Bay K8644 (1 μM), an L-type agonist, only boosted the current in some patches. The toxin blockers ω -conotoxin GVIA (1 μM), which fully blocks N-type channels (IUPHAR/BPS, 2015), or ω -agatoxin IVA (30 nM), which is reported to fully block P-type channels, did not affect the current. We did not test concentrations of ω -agatoxin IVA which would be required to block Q-type channels ($K_d = 100\text{-}200$ nM, see Catterall *et al.*, 2005). The activation threshold of the current was much more depolarized than typical for T-type channels. Our results differ somewhat from those of a previous study by Almog and Korngreen (2009), who also examined the pharmacology of calcium currents in nucleated patches from neocortical L5 pyramidal neurons, but using barium as the permeant ion. They also found no T-type channels, but did report the presence of all other subtypes, L-, N-, R-, P- and Q-types. In their hands, nifedipine, ω -conotoxin GVIA, ω -agatoxin IVA, as well as ω -conotoxin MVIIC (blocks Q-, N- and P-type) and SNX-482 (may block R-type) all blocked fractions of the current. Magee and Johnston (1995) studied Ca^{2+} channels in dendrites and somata of hippocampal pyramidal neurons, again with barium as the permeant ion. In dendrites, consistent with the results reported here, they find only occasional L-type channels, but predominantly a class of HVA medium conductance channels which they tentatively identify with R-type, based on the resistance of the channels to ω -conotoxin MVIIC. However, in somata, they found ω -conotoxin MVIIC to have a significant blocking effect, and they frequently encountered LVA T-type channels. The reasons for these

discrepancies are not clear, and may well partly be due to our use of physiological calcium as the permeant ion, and the different cell type studied by Magee and Johnston. Nevertheless, the voltage-dependence, pharmacological profile and the single exponential component of the autocorrelation of fluctuations suggest a reasonably homogeneous population of high-voltage-activated channels being activated under our conditions.

Comparison with previous estimates

The calcium concentration in the cerebrospinal fluid of rats is 1.0 to 1.5 mM (Jones & Keep, 1988; see also note in Weber *et al.*, 2010), while a standard value for artificial cerebrospinal fluid recipes that is often used in brain slice experiments (e.g. Stuart & Sakmann, 1994; Schiller *et al.*, 1997) is 2 mM. As for the single channel current in extracellular barium i_{Ba} , i_{Ca} depends on the calcium channel subtype, but there is no uniform ratio between i_{Ba} and i_{Ca} . T-type channels produce about the same current in barium and in calcium, whereas L-type and N-type channel currents are larger in barium (Fox *et al.*, 1987b). Hence the recognised hierarchy of single channel currents in barium, Cav1 (L-type) > Cav2 (N,P,Q,R-type) > Cav3 (T-type), is not valid in calcium. Weber *et al.* (2010) measured i_{Ca} for L-, N- and T-type channels and obtain the current hierarchy N-type > L-type > T-type, with the N-type current 38% larger than the L-type current, and the T-type current 16% smaller than the L-type current.

i_{Ca} does not depend linearly on the extracellular calcium concentration $[Ca^{2+}]_o$ or on the membrane voltage. i_{Ca} saturates at high $[Ca^{2+}]_o$ and the dependence can be described with the Hill equation (see discussion in Weber *et al.*, 2010). The voltage-dependence of i_{Ca} follows the nonlinear Goldman-Hodgkin-Katz current equation (Hille, 2001 p.445ff). Therefore, we restrict our comparison to i_{Ca} values at the same extracellular calcium concentration and membrane voltages, rather than comparing slope conductances. Fenwick *et al.* (1982) studied calcium channels in bovine adrenal chromaffin cells. In these cells, half of the calcium current is thought to flow through P/Q-type channels, and the other half through N- and also L-type channels (reviewed in Garcia *et al.*, 2006). At a membrane potential of -12 mV, fluctuation analysis yielded a single channel current of 0.03 pA in 1 mM Ca^{2+} and 0.09 pA in 5 mM Ca^{2+} , which is in good agreement with our results (0.04 pA in 1 mM Ca^{2+} , 0.11 pA in 5 mM). Gollasch *et*

al. (1992) studied L-type calcium channels in arterial smooth muscle and prolonged channel openings with BayK8644, which resulted in channel open times of 10 ms and longer, allowing filtering at 500 Hz. In cell-attached recordings in 2 mM $[Ca^{2+}]$, they obtained 0.10 pA at -20 mV and 0.20 pA at -40 mV. Compared with our almost constant value of 0.07 pA in the range between -20 and -40 mV, however, their current-voltage relationship is much steeper. In fact, extrapolating their values beyond -20 mV predicts a reversal potential of about 0 mV, although E_{Ca} should be highly positive. Taking into account that our currents are probably due to $Cav2$ channels and should hence be about 40% larger than L-type currents under otherwise equal conditions, the values in Gollasch *et al.* seem comparatively large. Weber *et al.* (2010) also used a direct single-channel recording approach, reducing noise by using quartz pipettes, and like Gollasch *et al.*, arrive at larger values than the ones reported here. For N-type channels in 2 mM Ca^{2+} , they obtain 0.21 pA at -25 mV. Compared with our value of 0.068 pA, this is about a factor of 3 larger. Part of the discrepancy may be due to different channel subtypes present in layer 5 pyramidal neurons. For example if R-type channels heavily contribute, they might have a smaller i_{Ca} than N-type channels, despite both being members of the $Cav2$ family. L-type channels may also contribute, which Weber *et al.* report to have a slightly smaller i_{Ca} .

Thus, single channel current estimates obtained by direct single-channel recordings appear to yield larger values than fluctuation analysis. When trying to judge by eye the size of a single channel current step at a low signal-to-noise ratio, close to the resolution limit, there is a danger of overestimating the single-channel current, if only a small subset of events are large enough to detect, or if insignificant fluctuations are mistaken for channel openings (see discussion in Weber *et al.*, 2010). Fenwick *et al.* (1982) compared single-channel currents in 95 mM Ba obtained by single-channel recordings with fluctuation analysis, and also obtained about 40% larger values in direct single-channel recordings. As a possible reason, they discuss a loss of noise power due to filtering, which reduces the single-channel current estimate from fluctuation analysis. However, we fully corrected for the effects of filtering, so this should not be an issue. Fenwick *et al.* also identified the possibility of heterogeneity in the channel population, i.e. that small channel openings can be missed by direct single-channel recordings but are picked up by fluctuation analysis.

Functional implications

In computational models of ion channels, it is usual to consider the limit of many ion channels, leading to deterministic differential equations for neuronal dynamics (Koch, 1999). Increasingly, though, it is appreciated that the stochastic current fluctuations due to the opening and closing of individual ion channels are not negligible, for example they can lead to spontaneous action potentials and have a large effect on action potential timing (Chow & White, 1996). Anwar *et al.* (2013) performed a detailed computational study of stochastic calcium spikes in cerebellar Purkinje cell dendrites, and found that large variability in calcium spike bursts, also seen experimentally, is produced in their model by the interaction of stochastic calcium influx with downstream calcium-dependent conductances, via stochastic intracellular calcium transport and buffering. Anwar *et al.* assumed a single channel permeability of $2.5 \times 10^{-5} \mu\text{m}^3 \text{ms}^{-1}$ for P-type channels, resulting in a single channel current of about 0.035 pA (at body temperature, 2 mM extracellular calcium and -50 mV membrane voltage), which is close to our values for 1 mM extracellular calcium.

The extreme sensitivity of calcium nanodomain concentrations to the calcium influx (Tadross *et al.*, 2013) means that downstream biochemical signalling is also critically dependent on the exact value of i_{Ca} . For example, stochastic calcium influx is predicted to have a major effect on CaMKII activation in dendritic spines (Zeng & Holmes, 2010) and therefore potentially on long-term potentiation. Although some of this calcium enters through NMDA receptors, dendritic calcium channels will also contribute, and therefore their physiological unitary properties, as well as those of NMDA receptors, are relevant in this regard.

To our knowledge, there have been no studies which directly recorded single voltage-gated calcium channels in physiological calcium concentration in the apical dendrite of layer 5 pyramidal neurons. Based on current-clamp and ionic substitution and blocker experiments, it has been suggested that there may be a “hot spot” of Ca^{2+} channel density at the dendritic Ca^{2+} spike initiation zone (see Larkum *et al.*, 2009; Perez-Garci *et al.*, 2013). It is conceivable that the subtype composition of dendritic calcium channels is different to that in the soma, but in the absence of further evidence, our data give the best available indication of the physiological single-channel current amplitude in the dendrite as well as the soma. In conclusion, by adapting and refining a

fluctuation analysis approach, we have been able to provide an improved estimate of the single channel current i_{Ca} of Ca^{2+} channels in physiological levels of extracellular Ca^{2+} , a quantity which has rarely been measured, despite its importance for stochastic single-channel effects or calcium nanodomains, as well as the timescale of autocorrelation of calcium channel gating. These results should assist in building more realistic computational models to understand calcium-dependent signalling in neurons.

References

- Almog M & Korngreen A (2009). Characterization of voltage-gated Ca^{2+} conductances in layer 5 neocortical pyramidal neurons from rats. *PLoS ONE* **4**, e4841.
- Anwar H, Hepburn I, Nedeleescu H, Chen W & De Schutter E (2013). Stochastic calcium mechanisms cause dendritic calcium spike variability. *J Neurosci* **33**, 15848–15867.
- Bean BP (1992). Whole-cell recording of calcium channel currents. *Meth Enzym* **207**, 181–193.
- Cannon RC, O'Donnell C & Nolan MF (2010). Stochastic ion channel gating in dendritic neurons: morphology dependence and probabilistic synaptic activation of dendritic spikes. *PLoS Comput Biol* **6**, e1000886, 1–18.
- Catterall WA, Perez-Reyes E, Snutch TP & Striessnig J (2005). International Union of Pharmacology. XLVIII. Nomenclature and structure-function relationships of voltage-gated calcium channels. *Pharmacol Rev* **57**, 411–425.
- Chow CC & White JA (1996). Spontaneous action potentials due to channel fluctuations. *Biophys J* **71**, 3013–3021.
- Church PJ & Stanley EF (1996). Single L-type calcium channel conductance with physiological levels of calcium in chick ciliary ganglion neurons. *J Physiol* **496** (Pt 1), 59–68.
- Davie JT, Kole MHP, Letzkus JJ, Rancz EA, Spruston N, Stuart GJ & Häusser M (2006). Dendritic patch-clamp recording. *Nat Protoc* **1**, 1235–1247.
- Fenwick EM, Marty A & Neher E (1982). Sodium and calcium channels in bovine chromaffin cells. *J Physiol* **331**, 599–635.
- Fox AP, Nowycky MC & Tsien RW (1987a). Single-channel recordings of three types of calcium channels in chick sensory neurones. *J Physiol* **394**, 173–200.

Fox AP, Nowycky MC & Tsien RW (1987b). Kinetic and pharmacological properties distinguishing three types of calcium currents in chick sensory neurones. *J Physiol* **394**, 149–172.

Garcia AG, Garcia-De-Diego AM, Gandia L, Borges R & Garcia-Sancho J (2006). Calcium signaling and exocytosis in adrenal chromaffin cells. *Physiol Rev* **86**, 1093–1131.

Gollasch M, Hescheler J, Quayle JM, Patlak JB & Nelson MT (1992). Single calcium channel currents of arterial smooth muscle at physiological calcium concentrations. *Am J Physiol* **263**, C948–C952.

Hille B (2001). *Ion Channels of Excitable Membranes*, 3rd edn. Sinauer.

IUPHAR/BPS (2015). *Guide to Pharmacology: Voltage-gated calcium channels*.

Available at:

<http://www.guidetopharmacology.org/GRAC/FamilyDisplayForward?familyId=80>
(accessed 07/2015).

Jones HC & Keep RF (1988). Brain fluid calcium concentration and response to acute hypercalcaemia during development in the rat. *J Physiol* **402**, 579–593.

Koch C (1999). *Biophysics of Computation*. OUP.

Larkum ME, Nevian T, Sandler M, Polsky A & Schiller J (2009). Synaptic integration in tuft dendrites of layer 5 pyramidal neurons: a new unifying principle. *Science* **325**, 756–760.

Levis RA & Rae JL (1993). The use of quartz patch pipettes for low noise single channel recording. *Biophys J* **65**, 1666–1677.

Magee JC & Johnston D (1995). Characterization of single voltage-gated Na⁺ and Ca²⁺ channels in apical dendrites of rat CA1 pyramidal neurons. *J Physiol* **487**, 67–90.

Major G, Larkum ME & Schiller J (2013). Active properties of neocortical pyramidal neuron dendrites. *Annu Rev Neurosci* **36**, 1–24.

Neher E & Stevens CF (1977). Conductance fluctuations and ionic pores in membranes. *Annu Rev Biophys Bioeng* **6**, 345–381.

Nowycky MC, Fox AP & Tsien RW (1985). Three types of neuronal calcium channel with different calcium agonist sensitivity. *Nature* **316**, 440–443.

Paxinos G & Watson C (2009). *The Rat Brain in Stereotaxic Coordinates*, compact 6th edn. Academic Press/Elsevier.

Perez-Garci E, Larkum ME & Nevian T (2013). Inhibition of dendritic Ca²⁺ spikes by

GABAB receptors in cortical pyramidal neurons is mediated by a direct $G_{i/o}$ - $\beta\gamma$ -subunit interaction with Cav1 channels. *J Physiol* **591**, 1599–1612.

Robinson HP, Sahara Y & Kawai N (1991). Nonstationary fluctuation analysis and direct resolution of single channel currents at postsynaptic sites. *Biophys J* **59**, 295–304.

Sakmann B & Neher E eds. (1995). *Single-Channel Recording*, 2nd edn. Plenum Press.

Sather W, Dieudonne S, MacDonald JF & Ascher P (1992). Activation and desensitization of N-methyl-D-aspartate receptors in nucleated outside-out patches from mouse neurones. *J Physiol* **450**, 643–672.

Schiller J, Schiller Y, Stuart G & Sakmann B (1997). Calcium action potentials restricted to distal apical dendrites of rat neocortical pyramidal neurons. *J Physiol* **505**, 605–616.

Sigworth FJ (1977). Sodium channels in nerve apparently have two conductance states. *Nature* **270**, 265–267.

Sigworth FJ (1980). The variance of sodium current fluctuations at the node of Ranvier. *J Physiol* **307**, 97–129.

Spruston N (2008). Pyramidal neurons: dendritic structure and synaptic integration. *Nat Rev Neurosci* **9**, 206–221.

Stevens CF (1972). Inferences about membrane properties from electrical noise measurements. *Biophys J* **12**, 1028–1047.

Stuart GJ & Sakmann B (1994). Active propagation of somatic action potentials into neocortical pyramidal dendrites. *Nature* **367**, 69–72.

Stuart GJ, Spruston N & Häusser M (2008). *Dendrites*, 2nd edn. OUP.

Südhof TC (2013). Neurotransmitter Release: The Last Millisecond in the Life of a Synaptic Vesicle. *Neuron* **80**, 675–690.

Tadross MR, Tsien RW & Yue DT (2013). Ca^{2+} channel nanodomains boost local Ca^{2+} amplitude. *Proc Natl Acad Sci* **110**, 15794–15799.

Traynelis SF, Angus Silver R & Cull-Candy SG (1993). Estimated conductance of glutamate receptor channels activated during EPSCs at the cerebellar mossy fiber-granule cell synapse. *Neuron* **11**, 279–289.

Tsien RW & Barrett CF (2005). A Brief History of Calcium Channel Discovery. In *Voltage-Gated Calcium Channels*, Molecular Biology Intelligence Unit, pp. 27–47. Springer US. Available at: http://link.springer.com/chapter/10.1007/0-387-27526-6_3 [Accessed August 25, 2015].

Weber AM, Wong FK, Tufford AR, Schlichter LC, Matveev V & Stanley EF (2010). N-type Ca²⁺ channels carry the largest current: implications for nanodomains and transmitter release. *Nat Neurosci* **13**, 1348–1350.

Zeng S & Holmes WR (2010). The Effect of Noise on CaMKII Activation in a Dendritic Spine During LTP Induction. *J Neurophysiol* **103**, 1798–1808.

Additional information

Competing interests

None.

Author contributions

Experiments were performed at the Physiological Laboratory, Department of Physiology, Development and Neuroscience, University of Cambridge. C.S. and H.P.C.R. designed the experiments. C.S. performed the experiments and analysed the data. C.S. and H.P.C.R. performed the simulations and wrote the manuscript.

Funding

C.S. acknowledges funding by the German Academic Exchange Service (DAAD), the Biotechnology and Biological Sciences Research Council (BBSRC), the Cambridge European Trust (CET) and the Research Innovation Fund of the University of Freiburg.

Single Ca^{2+} channel current-voltage curve (without correction): $\tilde{I} = \tilde{m} \cdot U + \tilde{c}$

Corrected current-voltage curve: $I = m \cdot U + c$

Voltage range: -45 mV to -18 mV

$[\text{Ca}^{2+}]_o$	\tilde{m} [pA/mV]	\tilde{c} [pA]	$r(\tilde{c}, \tilde{m})$
1 mM	0.00009 ± 0.00020	-0.0203 ± 0.0052	0.97
2 mM	0.00012 ± 0.00016	-0.0336 ± 0.0042	0.97
5 mM	0.00041 ± 0.00019	-0.0573 ± 0.0050	0.97
$[\text{Ca}^{2+}]_o$	m [pA/mV]	c [pA]	$r(c, m)$
1 mM	0.00017 ± 0.00037	-0.038 ± 0.010	0.93
2 mM	0.00022 ± 0.00030	-0.0625 ± 0.0089	0.83
5 mM	0.00076 ± 0.00036	-0.107 ± 0.012	0.67

Table 1. Parameter values for the single Ca^{2+} channel current voltage relationship at different Ca^{2+} concentrations. At the extracellular calcium concentrations $[\text{Ca}^{2+}]_o$ of 1 mM, 2 mM and 5 mM, the slope m and intercept c of the fitted current (I) voltage (U) curves (see Fig. 5) are given together with parameter errors and the correlation $r(c, m)$ between c and m . The top set of values (\tilde{m}, \tilde{c}) correspond to the uncorrected single-channel current, as obtained from straight line fits to data like shown in Fig. 4D. The bottom set of values (m, c) take into account the correction factor γ (see text).

FIGURE LEGENDS

Figure 1. Voltage-gated Ca^{2+} channel currents in nucleated patches from L5 pyramidal neurons. A) Leak-subtracted inward voltage-gated Ca^{2+} channel current during a family of voltage steps from -70 mV to -40 , -30 , -20 , -10 , 0 mV. B) Three sequential current responses during a voltage ramp from a holding potential of -70 mV to 0 mV. During the initial part of the ramp, there is a linear leak current (indicated by gray lines; black open squares indicate the range of the straight-line fit, from 5 ms to 40 ms after ramp onset). From about -40 mV, an inward current develops. C) The inward current is eliminated 18 s after addition of extracellular Cd^{2+} (200 μM). D) Three example patches in which peak current was insensitive to nifedipine (30 μM), ω -conotoxin GVIA (CTX, 1 μM) and ω -agatoxin IVA (ATX, 30 nM). Red bars indicate wash-in period during which currents were not measured, black bars indicate the presence of blocker. Note the quite typical time course of rundown of the calcium channel current in panel (i).

Figure 2. Isolation of current fluctuations. A) A heuristic piecewise polynomial function with continuous derivative was fitted by least squares to individual leak-subtracted ramp responses. The function consisted of an initial flat segment, and two linear sections joined by cubic splines. The transition times $t_{1...4}$, gradients $m_{a,b}$ and intercepts $I_{a,b}$ were all free parameters. B) There were no systematic deviations of fits (green curve) from individual current traces. Green dots indicate the range of the fitted data. C) Current variance was computed over 5 ms time bins through the current response. Green curve indicates the mean current fit.

Figure 3: Correction for effects of filtering. A) Channel noise is dominated by a single exponential relaxation. Blue trace shows the autocorrelation of the signal computed over one time bin (bin 10), with baseline autocorrelation subtracted. The red curve shows the least-squares fit to a model of exponentially-relaxing fluctuations (single Lorentzian spectral component). Undershoot is caused by the high-pass filter. B) Mean channel open/burst time τ , the relaxation time constant of fluctuations, extracted by this procedure is plotted for multiple patches and time bins, as a function of membrane

potential. Green is 1 mM $[Ca^{2+}]$, blue is 2 mM and red is 5 mM. Filled circles with error bars are mean and standard error of the mean obtained from about five adjacent data points. τ values are concentrated in the range 0.2-0.8 ms. C) Illustration of the effect of the bandpass filtering in the frequency domain. $L(f)$ indicates the Lorentzian distributed power of the underlying current fluctuations (PSD: power spectral density). The combined effect on noise power of the low- and high-pass filter characteristics ($A(f)$ and $B(f)$ respectively) is shown as the curve $A(f)^2 \cdot B(f)^2$. Channel noise power which passes through filtering is shown in red: $L(f) \cdot A(f)^2 \cdot B(f)^2$. D) The ratio of the integral of the noise power density passed by the filter to the total noise power gives the correction factor γ , whose dependence on the noise relaxation time constant τ is shown as the solid curve, the combined effect of the low-pass filtering (dashed curve) and high-pass filtering (dotted curve). γ is quite insensitive to τ over the experimentally-relevant range. E) Using the same procedure of current fitting and filtering for synthetic data with exponentially correlated channel noise and baseline noise matching experimental conditions (100 trials), we show that the analysis faithfully recovers the underlying single channel current amplitude (analysis for bin 10; $\tau = 0.3$ ms; similar result at $\tau = 1$ ms, not shown). Solid line indicates equality. Error bars show the standard deviation of the single channel current estimates from single trials.

Figure 4. Fluctuation measurements in one patch. A) Scatter plot of current variance versus mean current, measured in the baseline bin. B) Same for bin 1 of the ramp (green points) relative to the baseline (black, same as in A, for comparison). Black line: straight line fit through the baseline and test bin data. The resulting slope estimate and its error are given. C) Same for bin 10. D) Plot of the obtained slope values, with error bars, corresponding to $\gamma \cdot i$, against bin voltage (γ : correction factor; i : single channel current). Straight line indicates error-weighted linear fit, predicting a highly positive reversal potential as expected for calcium channels.

Figure 5. Summary of single calcium channel current amplitude, at different membrane potentials and calcium concentrations. Data for 1 mM $[Ca^{2+}]_o$ in green (2 patches), 2 mM in blue (2 patches) and 5 mM in red (3 patches). Data from Fig. 4D are shown as blue filled circles. Different patches indicated by different symbols. Straight line fits of

the pooled data at each calcium concentration are shown. There is relatively weak voltage-dependence, but a large increase in single channel current amplitude with increasing extracellular calcium concentration.

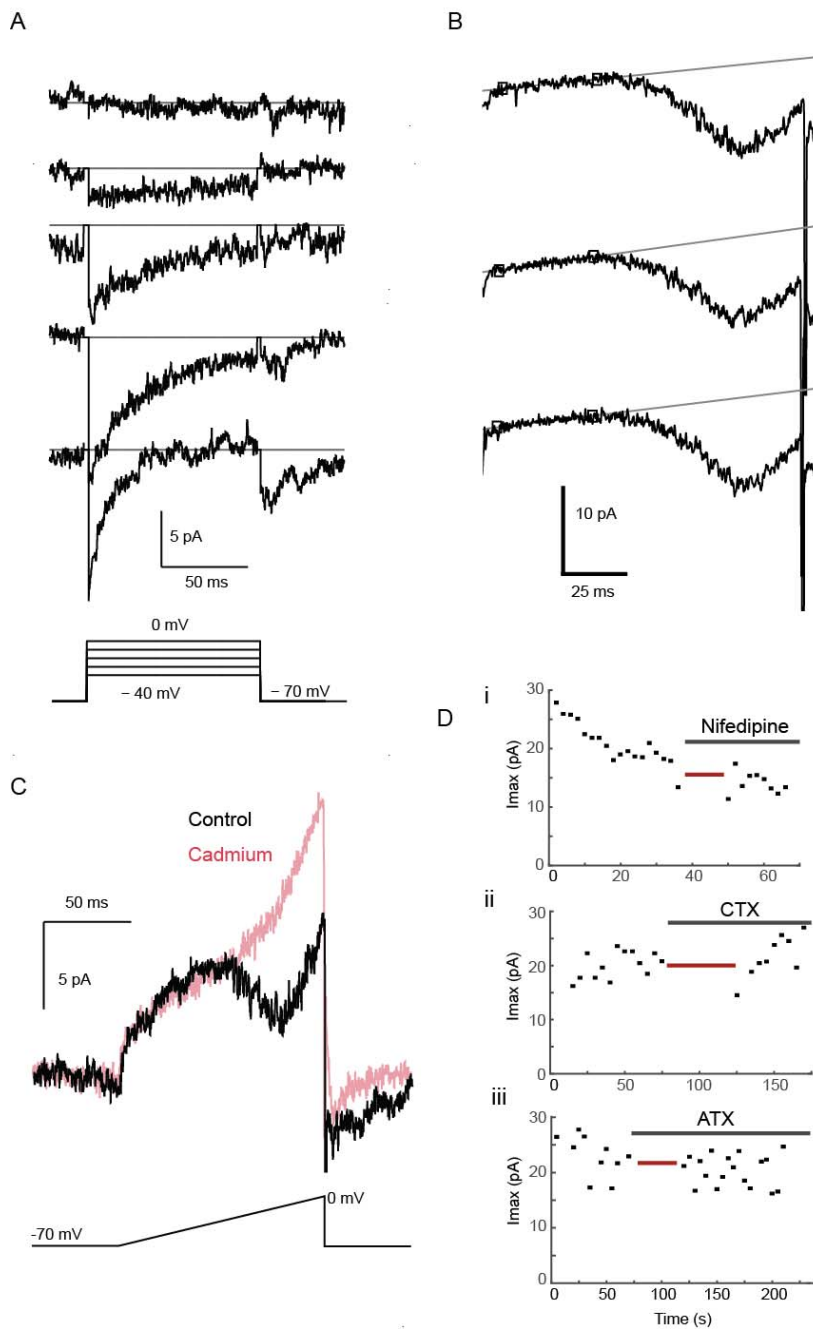


Figure 1

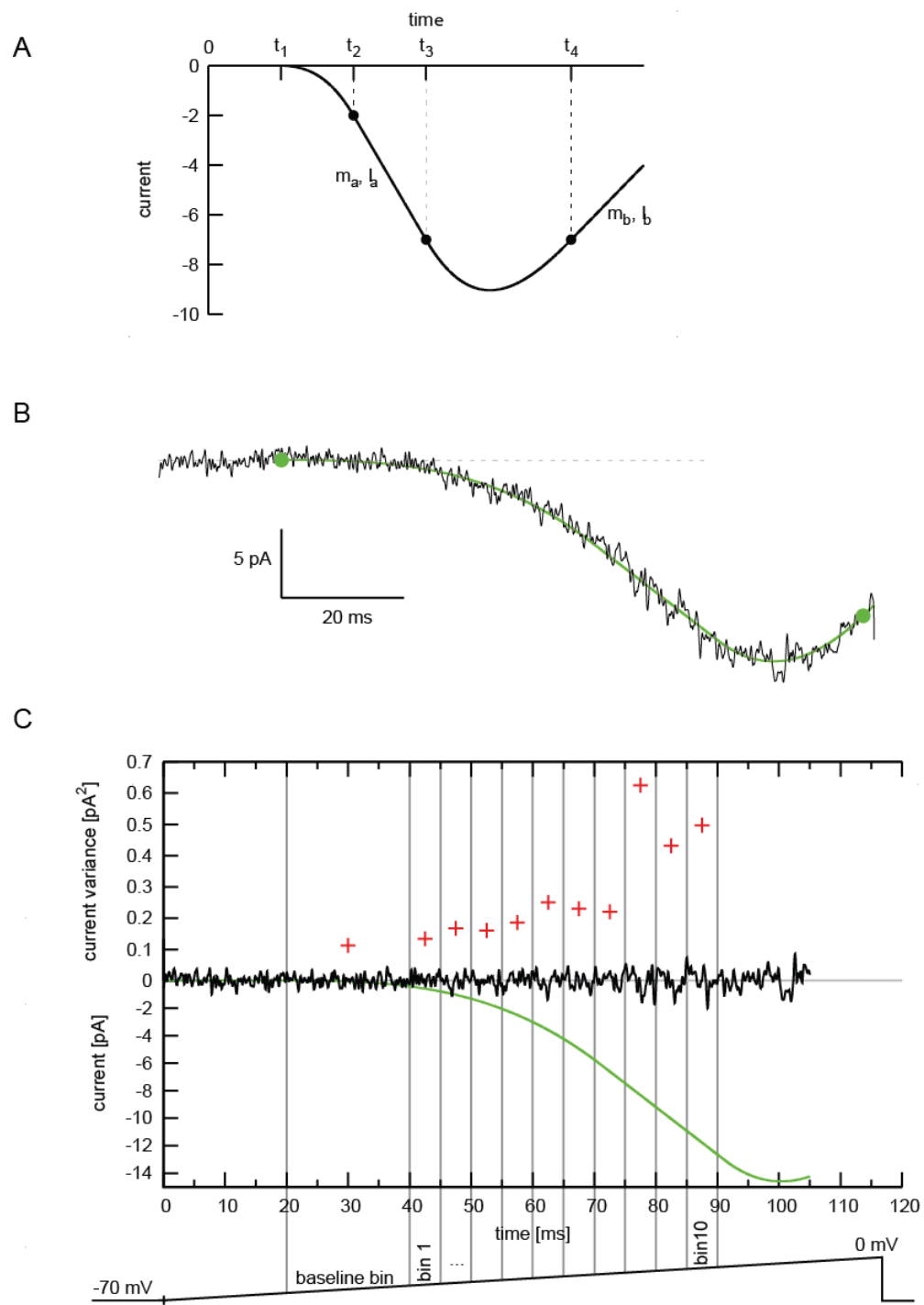


Figure 2

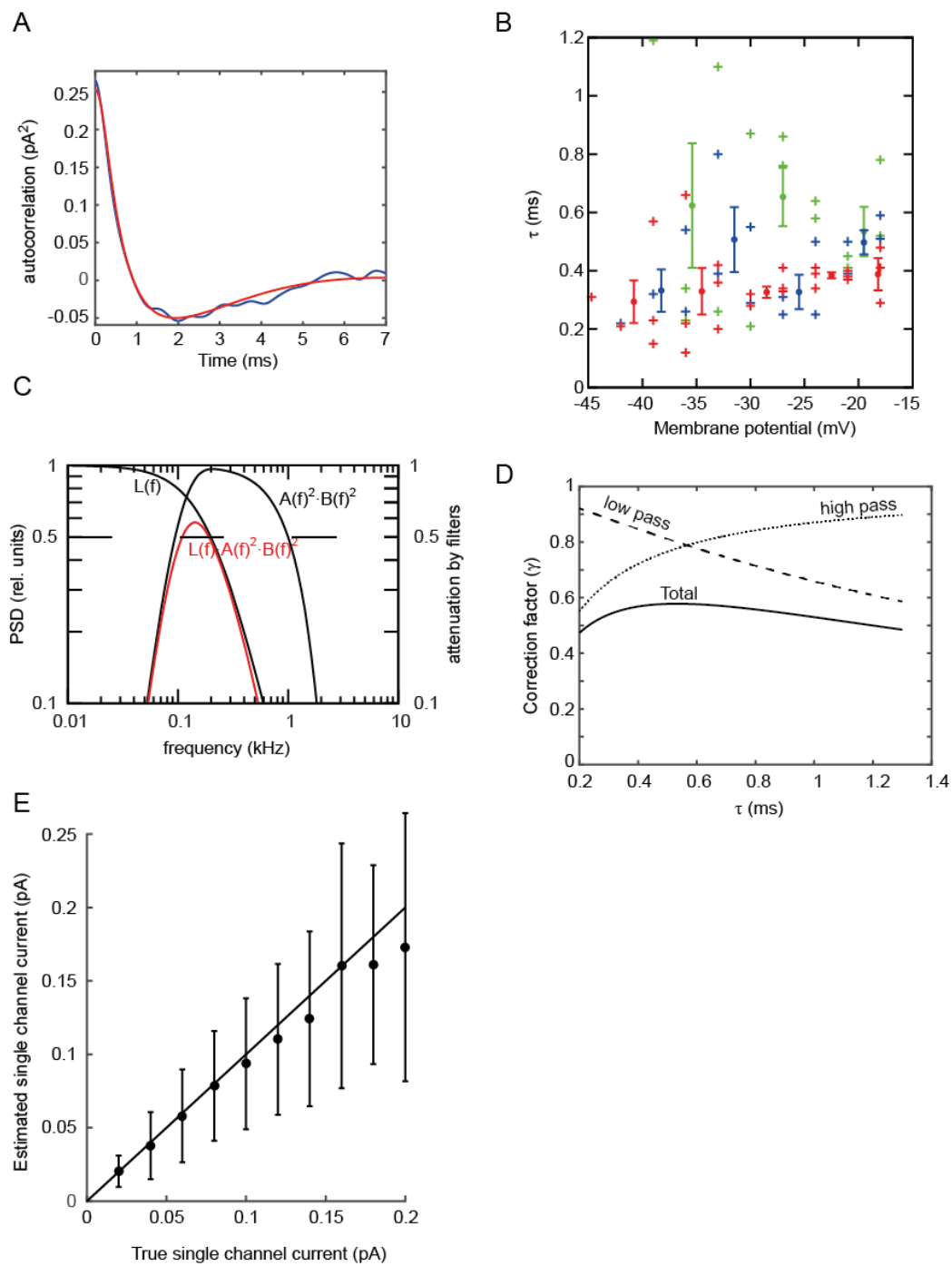


Figure 3

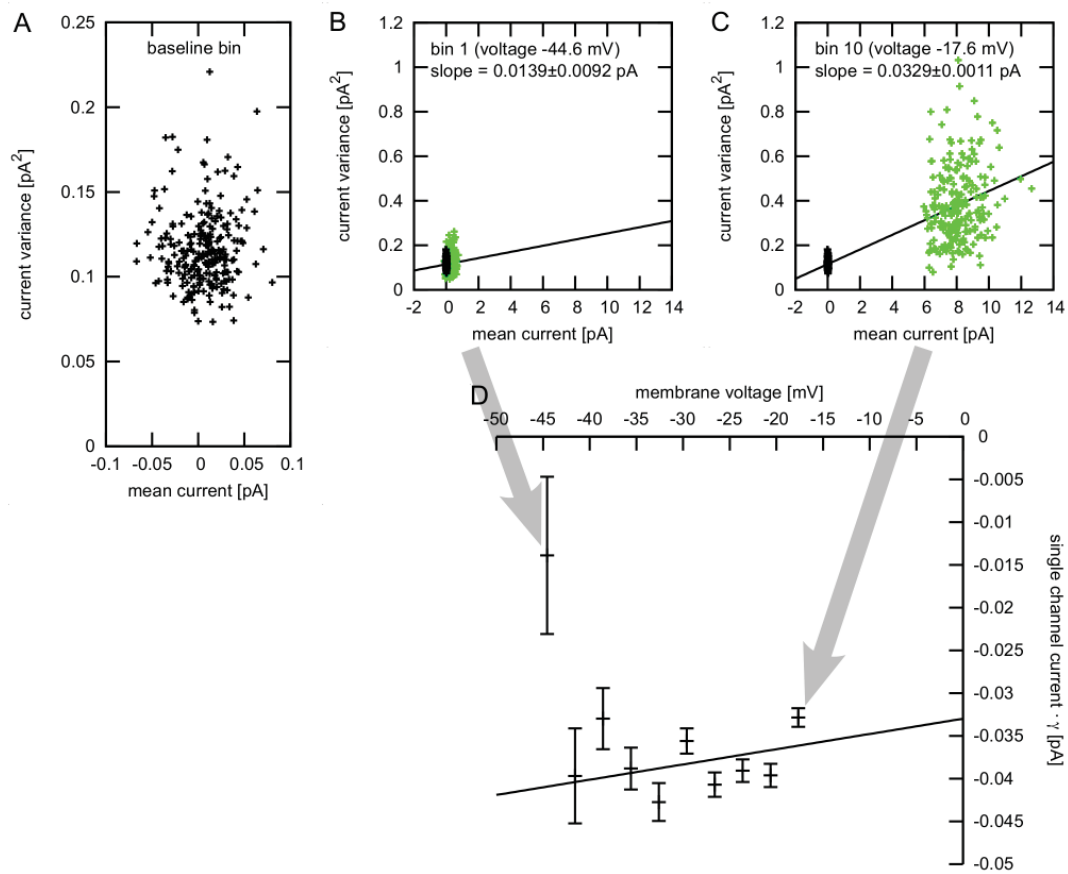


Figure 4

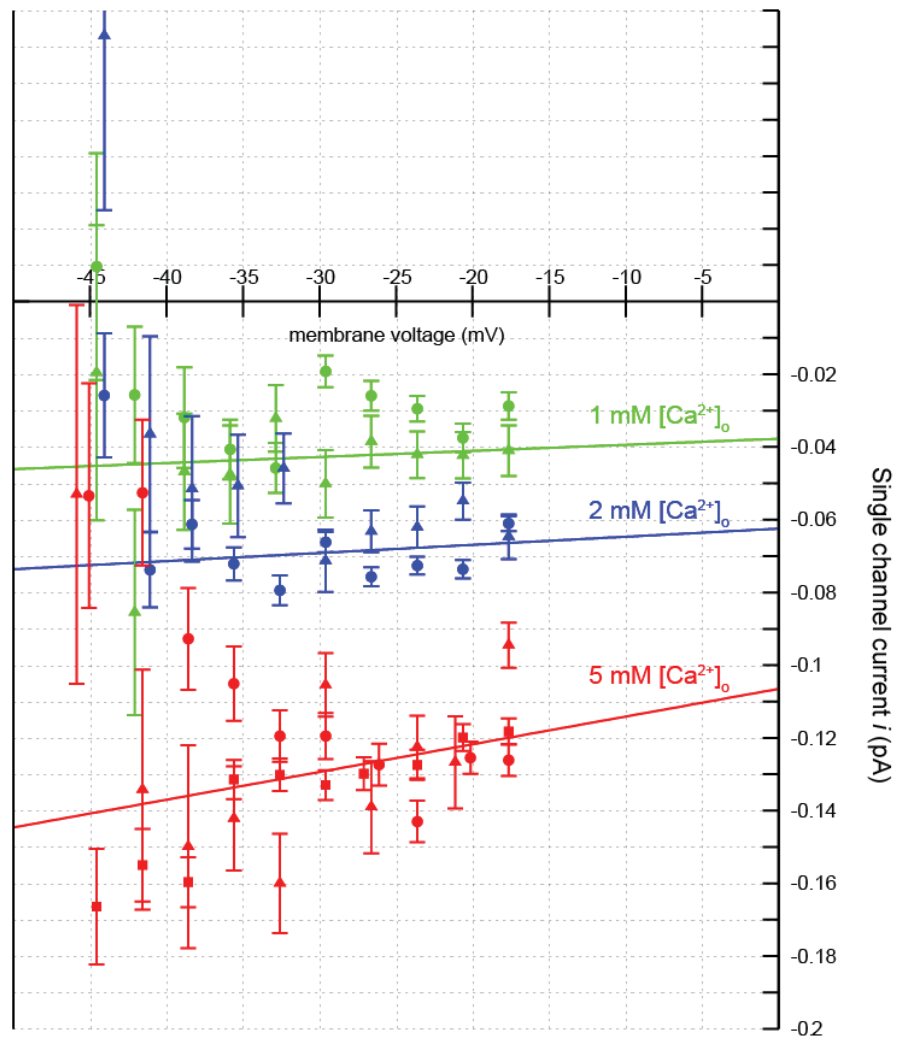


Figure 5